Geophysical Research Letters

RESEARCH LETTER
10.1029/2023GL104805

The Hydrologic Cycle and Atmospheric Rivers in CESM2 Simulations of the Last Glacial Maximum

J. M. Lora[1], C. B. Skinner[2], W. D. Rush[1,3], and S. H. Baek[1]

[1]Department of Earth and Planetary Sciences, Yale University, New Haven, CT, USA, [2]Department of Environmental, Earth and Atmospheric Sciences, University of Massachusetts Lowell, Lowell, MA, USA, [3]Cooperative Institute for Research in Environmental Sciences, University of Colorado Boulder, Boulder, CO, USA

Key Points:

- Average and extreme precipitation declined globally during the Last Glacial Maximum with three notable mid-latitude exceptions over land
- Moisture transport changes mainly caused by ice sheets, with lower CO_2 and altered insolation causing enhanced drying regionally
- Atmospheric river activity decreased globally except over the North Atlantic, where it enhanced precipitation over Iberia

Supporting Information:

Supporting Information may be found in the online version of this article.

Correspondence to:

J. M. Lora,
juan.lora@yale.edu

Citation:

Lora, J. M., Skinner, C. B., Rush, W. D., & Baek, S. H. (2023). The hydrologic cycle and atmospheric rivers in CESM2 simulations of the Last Glacial Maximum. *Geophysical Research Letters*, *50*, e2023GL104805. https://doi.org/10.1029/2023GL104805

Received 1 JUN 2023
Accepted 1 SEP 2023

Abstract Proxy reconstructions and model simulations of precipitation during Earth's glacial periods suggest that the locations and mechanisms of atmospheric moisture transport have changed considerably during Earth's past. We investigate the hydroclimate of the Last Glacial Maximum (LGM) using simulations with the Community Earth System Model, with a focus on the extratropics and the influence of atmospheric rivers (ARs), a key driver of modern-day moisture transport globally. Mean and extreme precipitation increase significantly over southwestern Patagonia, Iberia, and southwestern North America—mid-latitude regions affected by ARs in the modern climate—despite overall decreases elsewhere. In each, the associated moisture transport changes are different, with increased transport and AR activity mainly occurring in the North Atlantic. The overall LGM response is dominated by the response to ice sheets, with other forcings causing additional cooling and drying over the extratropics and a strong decrease of moisture transport over the subpolar North Atlantic.

Plain Language Summary During the last ice age, when glaciers reached their maximum extent, atmospheric CO_2 was lower and Earth's orbit was different. All of these influences caused dramatic changes in precipitation patterns around the planet. Using climate model simulations, we find that the majority of the changes to atmospheric moisture transport and precipitation patterns result from the presence of the ice sheets alone, with lower CO_2 and insolation differences enhancing the ice sheet-induced patterns. These changes mainly comprise decreases in moisture transport and lower precipitation, with three notable exceptions in Patagonia, Iberia, and southwestern North America. Of these, precipitation increases over Iberia result from increased transport by plumes of moisture, known as atmospheric rivers , across the North Atlantic. Elsewhere in the world, AR activity decreases.

1. Introduction

The hydrologic cycle of the Last Glacial Maximum (LGM; ~21,000 years ago) has received considerable attention, particularly regarding changes relative to the modern in net precipitation over land (Amaya et al., 2022; Boos, 2012; Broecker, 2010; Kutzbach & Wright, 1985; Lora, 2018; Lora et al., 2017; Morrill et al., 2018; Scheff et al., 2017; Tabor et al., 2021). There is evidence from various regions that, despite a much colder global climate (i.e., Annan et al., 2022; Paul et al., 2021; Tierney et al., 2020), significant increases in local precipitation occurred at the LGM, contrary to simple thermodynamic expectations (see Boos, 2012), especially along the western extratropical portions of continents (Beghin et al., 2016; Goldsmith et al., 2017; Kirby et al., 2013; Oster et al., 2015). Given that changes in the atmospheric circulation have been found to be critical to changes of the moisture budget (Boos, 2012; Lora, 2018; Morrill et al., 2018), the response of the transport of moisture to LGM forcings and its connections to these increases (and changes elsewhere) are thus important considerations for understanding the LGM hydroclimate.

In addition to lower greenhouse gas concentrations and a slightly altered insolation distribution, the LGM featured large ice sheets whose presence substantially altered the atmospheric circulation and climate system. Stationary waves excited by the ice sheets' topography and albedo have been variously linked to changes in the locations, tilts, intensity, and variability of the mid-latitude jets, and associated extratropical precipitation distributions (Amaya et al., 2022; Cook & Held, 1988; Lee et al., 2023; Lofverstrom, 2020; Löfverström et al., 2016; Merz et al., 2015; Roberts et al., 2019). Similarly, many studies have investigated the dynamics of transient eddies (extratropical cyclones) and the storm tracks, and their (potentially model-dependent) responses to the ice sheets

and steepened LGM meridional temperature gradients (Donohoe & Battisti, 2009; Kageyama & Valdes, 2000; Laîné et al., 2009; Li & Battisti, 2008; Pinto & Ludwig, 2020; Rivière et al., 2010, 2018). Importantly, ice sheet reconstructions remain uncertain, with impacts on the strength of the response of the circulation (Kageyama et al., 2021; Merz et al., 2015; Ullman et al., 2014). Yet, aside from a few studies with a regional purview (Lofverstrom, 2020; Lora et al., 2017; Tabor et al., 2021), most such previous investigations have not provided much detail about the transport of moisture by the atmosphere.

In this study, we investigate the response of moisture transport (and its convergence), which incorporates both circulation and humidity changes (e.g., O'Gorman & Schneider, 2008), to LGM conditions, with an emphasis on the influences exerted by the ice sheets. An important aim is a better understanding not just of the behavior of the disturbances that lead to precipitation, but also of the provenance of the moisture comprising this precipitation. We are also motivated to examine the statistical extremes of precipitation and moisture transport events, as these have previously been implicated as important contributors to the local LGM hydroclimate of western North America and Europe (Lofverstrom, 2020; Lora et al., 2017). In the present day, these regions are heavily influenced by atmospheric rivers (ARs), synoptic plumes of water vapor that account for the majority of atmospheric moisture transport and are associated with extreme precipitation (high intensity precipitation events; Dettinger et al., 2011; Guan et al., 2010; Lamjiri et al., 2017; Lavers & Villarini, 2013; Ralph et al., 2019; Waliser & Guan, 2017; Zhu & Newell, 1998). Yet modern-day ARs occur across all of the extratropics in close connection with the storm tracks (Baek et al., 2023; Lora et al., 2020; Newman et al., 2012; Shaw et al., 2016; Sodemann & Stohl, 2013; Viale et al., 2018; Zhang et al., 2019; Zhu & Newell, 1998); therefore, whether and to what extent LGM ice sheet and other forcings alter the behavior of ARs globally is our primary interest. A companion study (Skinner et al., 2023) investigates the influence of ARs on the LGM ice sheets themselves; our focus here is on the unglaciated mid-latitudes.

2. Methods

We use three sets of simulations with the Community Earth System Model version 2 (CESM2) (Danabasoglu et al., 2020), as in Skinner et al. (2023) (Text S1 in Supporting Information S1). Briefly, these comprise a preindustrial control simulation, a full LGM simulation (including lower greenhouse gas concentrations and modified insolation), and a simulation with LGM ice sheets but otherwise the same as preindustrial. In all cases, the simulations use a model horizontal resolution of $0.9° \times 1.25°$ for the atmosphere/land and 1° for the ocean/sea ice. In the two relevant cases, the LGM ice sheet is prescribed using the ICE-6G reconstruction at 21 ka (Peltier et al., 2015). Our results are based on 100 years of simulation after a period of spin-up (Text S1 in Supporting Information S1). All differences between simulations shown below display only significant results ($p < 0.01$) using a two-sided *t*-test.

We define extreme precipitation as the value of precipitation at the all-interval 99th percentile locally (Schär et al., 2016), using 6-hourly precipitation; therefore, comparisons between simulations show the change in that value (rather than a percentile change for a given value). We identify ARs using the algorithm ("Lora_v2") described in Skinner et al. (2020, 2023). ARs are defined from 6-hourly integrated vapor transport (IVT) regions that exceed a threshold value, which depends on the 30-day running mean of the zonally averaged integrated water vapor, thus accounting both for latitudinal gradients in moisture and also for the background climate state; this enables comparisons across different or changing climates (Baek & Lora, 2021; Baek et al., 2023; Menemenlis et al., 2021; O'Brien et al., 2022; Skinner et al., 2020; Skinner et al., 2023). Within the modern climate, the algorithm compares favorably with most other detection methods, particularly for moderate (i.e., wherein IVT roughly exceeds 500 kg m^{-1} s^{-1}) and stronger ARs (Lora et al., 2020; Marquardt Collow et al., 2022; Rutz et al., 2019). Finally, for our purposes, AR IVT and AR precipitation are defined simply as IVT and precipitation that are concurrent with AR regions.

3. Results

3.1. Precipitation and Moisture Transport

Globally, average precipitation changes at the LGM in our simulations are primarily comprised of tropical and extratropical drying accompanied by wetting over subtropical oceans, in agreement with the PMIP4 model ensemble (Kageyama et al., 2021) and as might be expected from a simple thermodynamic scaling (compare

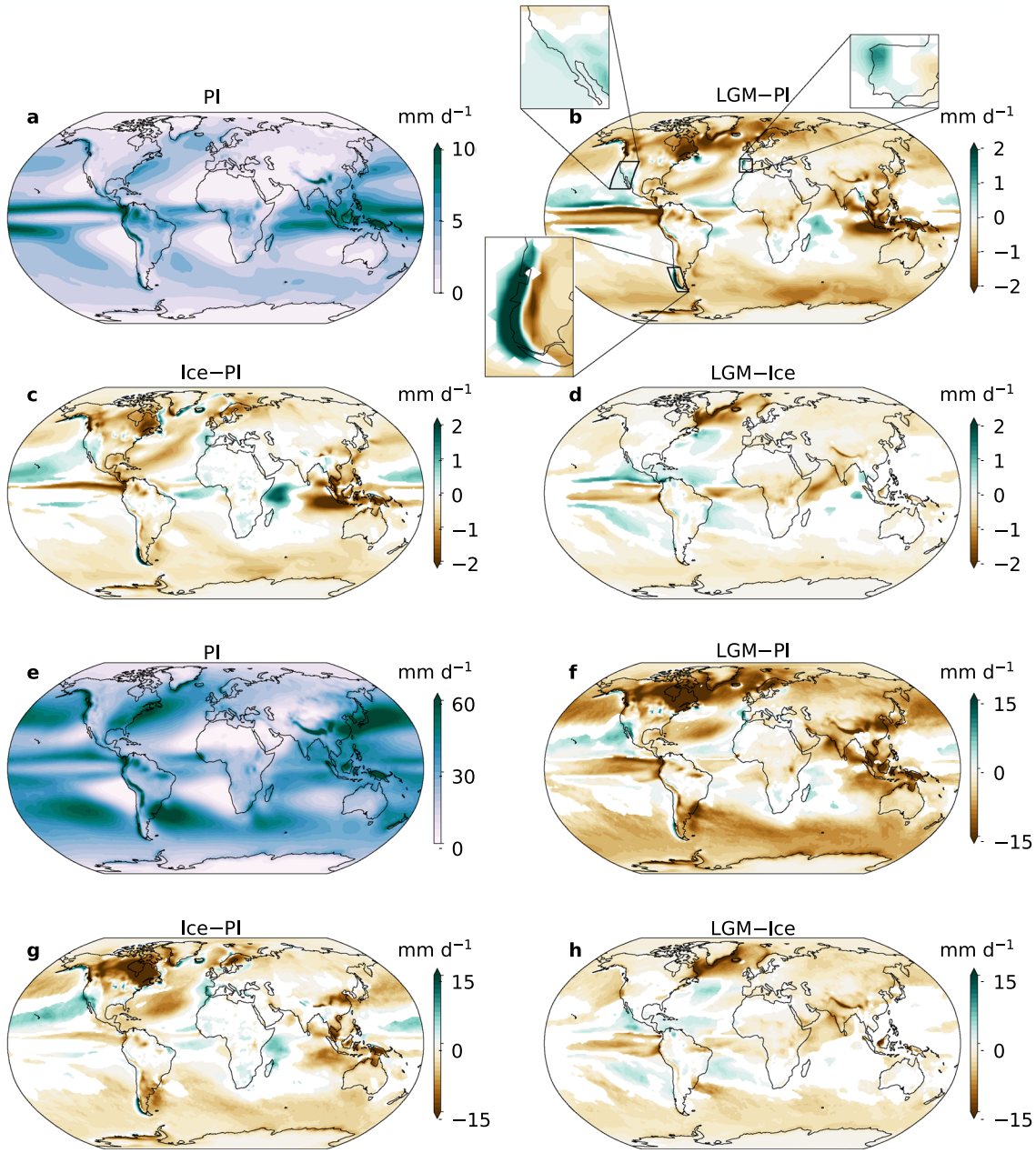

Figure 1. Average and extreme precipitation. (a) Average precipitation from the preindustrial simulation, and the differences in precipitation between (b) full LGM and preindustrial simulations, (c) LGM ice sheet and preindustrial simulations, and (d) full LGM and LGM ice sheet simulations. Insets in panel (b) highlight three regions of interest. (e–h) Extreme precipitation defined as the local values of the 99th percentile precipitation; panels as in (a)–(d).

Figures 1a and 1b; Held & Soden, 2006). Over land, most regions see a decrease in precipitation, with a few notable exceptions (Figure 1b; see insets): there are large increases (>1 mm d^{-1}) in northwestern Iberia and the Patagonian Andes, along with smaller but significant increases in southwestern North America, eastern and western Amazonia, parts of southern and the northwestern coast of Africa, northern Madagascar, and Myanmar.

Many of these increases, particularly in the mid-latitudes, are associated with increases due to the presence of continental ice sheets (Figures 1c and 1d); the differences in the precipitation responses between LGM and ice-sheet simulations are concentrated near the tropics, and over the North Atlantic where substantial sea ice differences (due to the colder LGM climate) modify the atmospheric circulation. Elsewhere, the response can be interpreted as a modest overall drying on top of the response to the ice sheets (Figure 1d). This is particularly

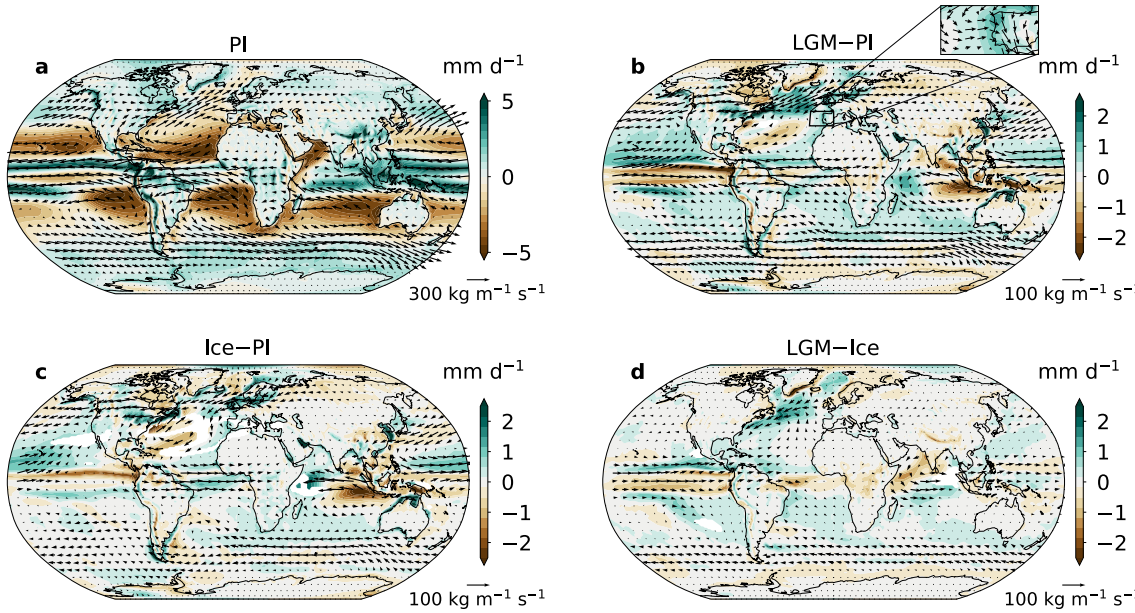

Figure 2. Atmospheric moisture transport and its convergence. Average atmospheric integrated vapor transport (IVT; arrows) and IVT convergence (filled contours). Panels as in Figures 1a–1d. In the inset (panel b), IVT arrows are enlarged by a factor of four relative to the key.

so in the three western mid-latitude coastal regions experiencing significant precipitation increases, which are therefore clearly linked to the ice sheet forcing in particular. Importantly, we find no large changes in the seasonality of precipitation except over the maritime continent and over the northern hemisphere ice sheets and Arctic Ocean, where in both cases the proportion of summertime precipitation increases (Text S2, Figures S1 and S2 in Supporting Information S1). This indicates that the provenance and mechanisms of precipitation in the extratropics are not significantly different between LGM and preindustrial climates.

Changes in extreme precipitation follow similar patterns as average precipitation; notably, large increases in 99th percentile precipitation (>10 mm d^{-1}) occur over southwestern North America, western Iberia, and western Patagonia (Figure 1f), three mid-latitude regions sensitive to AR activity in the modern. All three of these regional increases are entirely due to the ice sheet forcing; that is, they occur in the ice-sheet simulation and there is little difference in the response between that and the full LGM simulation (Figures 1g and 1h). We note that, while in Patagonia increased precipitation occurs over higher ice sheets that enhance topographic and temperature gradients, explaining the increase in average and extreme precipitation on the western slopes, the enhancements over the two other regions require other explanations like changes in moisture delivery. Over most other regions of the globe, extreme precipitation decreases substantially (Figure 1f), and the difference in response between LGM and ice-sheet simulations resembles that of average precipitation (Figure 1h).

We next examine moisture transport and its extremes. Annual average moisture transport in the preindustrial largely consists of easterly fluxes in the tropics, anticyclonic patterns over ocean basins between the subtropics and extratropics, and westerly transport at high mid-latitudes, including onto continents (Figure 2a). These transport patterns are associated with meridional convergence of moisture in the intertropical convergence zone (ITCZ), divergence over the subtropical oceans where evaporation outpaces precipitation, and broad but more modest convergence in the extratropics, which peaks over land along coastlines at these latitudes.

Broadly, the response at the LGM is a weakening of all of these patterns, but with varying magnitudes regionally (Figure 2b). This is due to a combination of changes to the circulation and column water vapor, which peak in different regions (Figures S3 and S4 in Supporting Information S1). Notably, many of the precipitation increases noted above result from increased atmospheric moisture convergence. This is particularly the case for Iberia and Patagonia, west of which average moisture transport is slightly strengthened and weakened, respectively (Figure 2b; see inset). On the other hand, over southwestern North America, moisture transport and convergence changes are small, and the LGM precipitation increases of up to 1 mm d^{-1} along northwestern Mexico are therefore accompanied by evaporation increases of similar magnitude (since net precipitation approximately balances

moisture convergence; e.g., Lora, 2018). Moisture transport into the continent from the western North Pacific generally decreases, except into Mexico, which sees small increases particularly from the south.

Interestingly, most of the moisture transport changes are associated with the ice sheet forcing (Figure 2c). Over mid-latitude land regions, this is consistent with previous results with PMIP2 and 3 that indicate the importance of dynamical relative to thermodynamic changes (e.g., Boos, 2012; Lora, 2018), though here the ice sheet forcing induces both circulation changes and decreases in column water vapor (Figures S3 and S4 in Supporting Information S1). The major exceptions, where other LGM forcings dominate, occur over the northern North Atlantic and the tropical Pacific and Indian Oceans (Figure 2d). The former is again linked to the presence of sea ice in the colder LGM simulation, which substantially weakens westerly moisture transport over the region. The tropical responses consist of a more complicated pattern in the LGM simulation wherein the Pacific ITCZ extends deeper into the northern hemisphere and the southern convergence zone extends farther toward south America, while in the Indian Ocean the ice sheet forcing induces an enhancement of easterly moisture transport across the basin that is moderated by a weakened Somali Jet in the full LGM simulation (see DiNezio et al., 2018). The differences in atmospheric moisture transport and moisture convergence between LGM and ice-sheet simulations are minor over land (Figure 2d).

3.2. Atmospheric Rivers

To better understand climatological changes associated with the synoptic patterns of greatest influence on mid-latitude moisture transport, and which are often associated with extreme precipitation over extratropical coastal land areas, we next examine AR activity in our simulations. In the preindustrial case, ARs occur primarily over the extratropical oceans (Figure 3a), in good agreement with previous results with reanalysis (e.g., Lora et al., 2020). Over land, AR frequency is highest over the eastern portions of extratropical continents, but westerly moisture transport by ARs into western North America, Europe, and southern South America is considerable. Substantial inland penetration of ARs is not obvious in the annual average, which results in part from rapid rainout of moisture over land that in turn limits their detectability there. The response of AR activity and its associated precipitation in the LGM simulation is comprised primarily of global weakening (Figure 3b): All of the AR tracks see mean reductions (on the order of 50 kg m^{-1} s^{-1}) of westerly and poleward moisture transport by ARs, and less AR precipitation (by upwards of 1 mm d^{-1}), with the notable exception of Iberia and the North Atlantic to its west.

Indeed, the response in the North Atlantic appears as a tripolar structure, with large reductions in the north, modest reductions around its subtropical latitudes, and a slight increase in AR frequency, moisture transport, and precipitation in the region in between. This pattern is the consequence of a southward displacement of storms by cold LGM conditions in the subarctic region, as well as a narrowing and zonalization of the North Atlantic atmospheric circulation (see also Figures S3 and S5 in Supporting Information S1). This is associated with the ice sheet forcing (Figure 3c), as expected from previous results (Löfverström et al., 2016; Löfverström & Lora, 2017; Merz et al., 2015), indicating that the ice sheet reconstruction employed elicits a strong response associated with high ice sheet topography. Ice sheet forcing alone causes increased AR moisture transport and precipitation between the east coast of North America and Iberia, due to a zonalization and constriction of the AR track there. The additional influence of other LGM forcings consists of general weakening (Figure 3d), which again is especially strong in the North Atlantic due to the enhanced polar cooling there (Figure S6 in Supporting Information S1). As a result, large LGM reductions (~50%) in AR frequency and accompanying decreases in precipitation occur over the British Isles and into northwestern Europe, accompanying the more subtle increases over western Iberia (Figure 3b).

Other mid-latitude land regions also see substantial reductions in AR frequency at the LGM, consistent with their reduced average and extreme precipitation (Figures 1b, 1f, and 3b). Over coastal east Asia (including all of Japan) and the Pacific Northwest of North America (where ARs provide 30%–40% of precipitation in the preindustrial; Figure 3e), AR activity decreases by roughly 50% at the LGM (Figure 3b); similar reductions occur over southern South Africa, southern Australia, and New Zealand in the southern hemisphere. Over eastern North America and southeastern South America, the reductions are even larger and extend far into each continent. For example, over the former, nearly all AR activity disappears; this is largely due to the presence of the ice sheet there (see Skinner et al., 2023).

In the preindustrial simulation, up to 75% of total precipitation along the centers of the AR tracks is due to ARs, as are similar percentages of extreme precipitation (Figure 3e). (Note that this far exceeds the frequency of ARs in

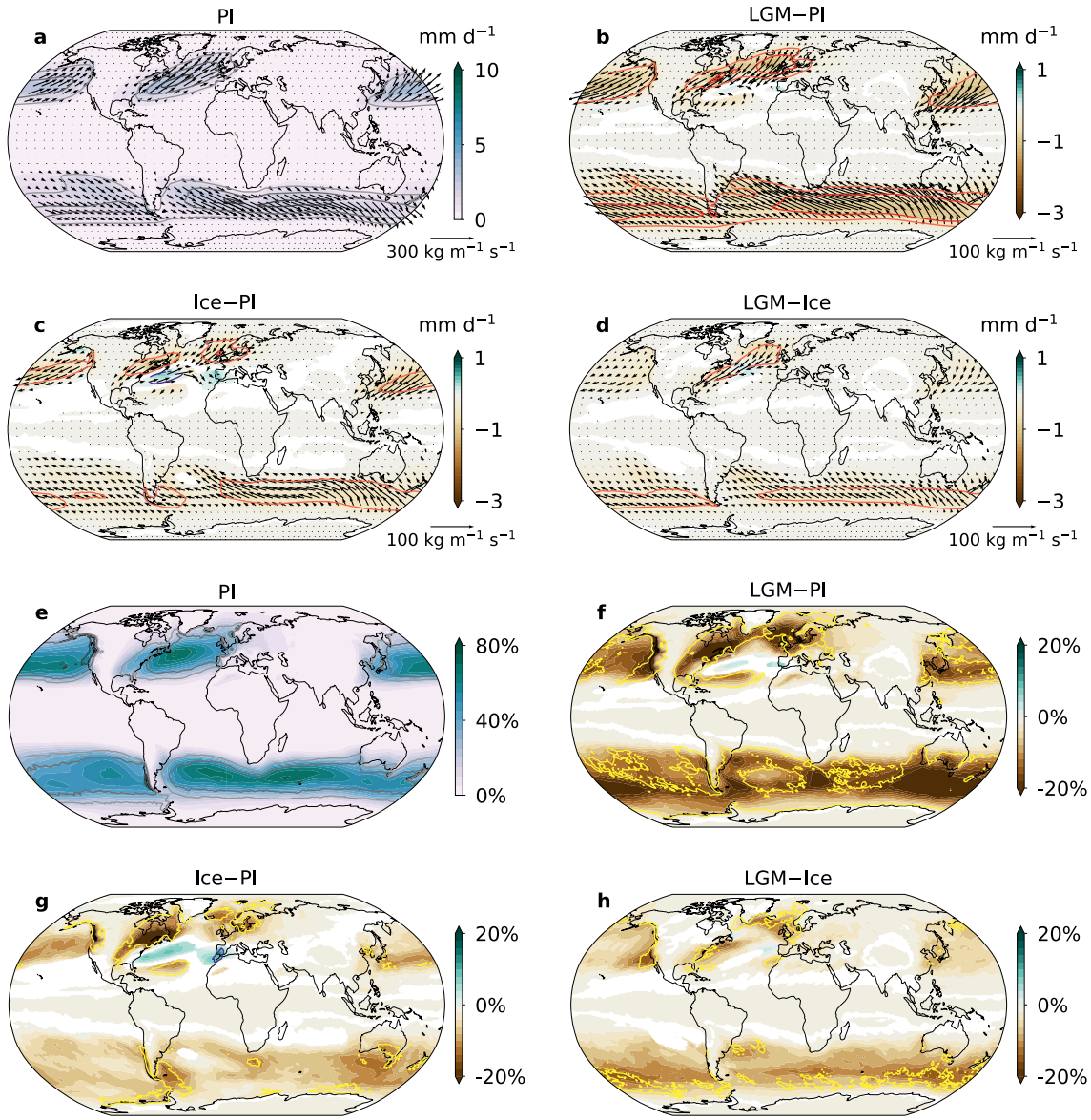

Figure 3. Atmospheric rivers (ARs). (a–d) Average frequency of AR occurrence (open contours; units are percentage of time steps with AR conditions; 10%, 20%, and 30% contours are shown in panel (a), and −10%, −5%, 5%, and 10% contours, from red to blue, in panels (b)–(d)), atmospheric moisture transport due to ARs (arrows), and precipitation associated with ARs (filled contours). Panels as in Figures 1a–1d. (e–h) Average percentage of total precipitation associated with ARs (filled contours) and average percentage of 99th percentile precipitation associated with ARs (open contours; 50%, 70%, and 90% contours are shown in panel (e), −15% (yellow) and +15% (blue) contours shown in panels (f)–(h)). Panels as in (a)–(d).

the same regions, indicating that ARs are important drivers of total and extreme precipitation.) Over land regions affected by ARs, the percentages of total and extreme precipitation associated with ARs are up to about 45% and well over 50%, respectively; indeed, over coastal areas of the Pacific Northwest, Patagonia, and northwestern Iberia, ARs account for more than 90% of extreme precipitation. In the LGM simulation, most regions see substantial decreases in these AR contributions, with, in particular, decreases of >20% (>15%) of total (extreme) precipitation over western and northeastern North America, the British Isles and Europe, Patagonia, and parts of New Zealand (Figure 3f). The decreased AR contributions are largest at the peripheries of the preindustrial AR tracks (compare Figures 3e and 3f), indicating that ARs contribute less to the water cycle of the LGM globally. The major exception is the region between North America and Iberia, which sees modest but significant increases in the AR fraction of total precipitation, coincident with the region where LGM AR frequency increases (Figure 3b).

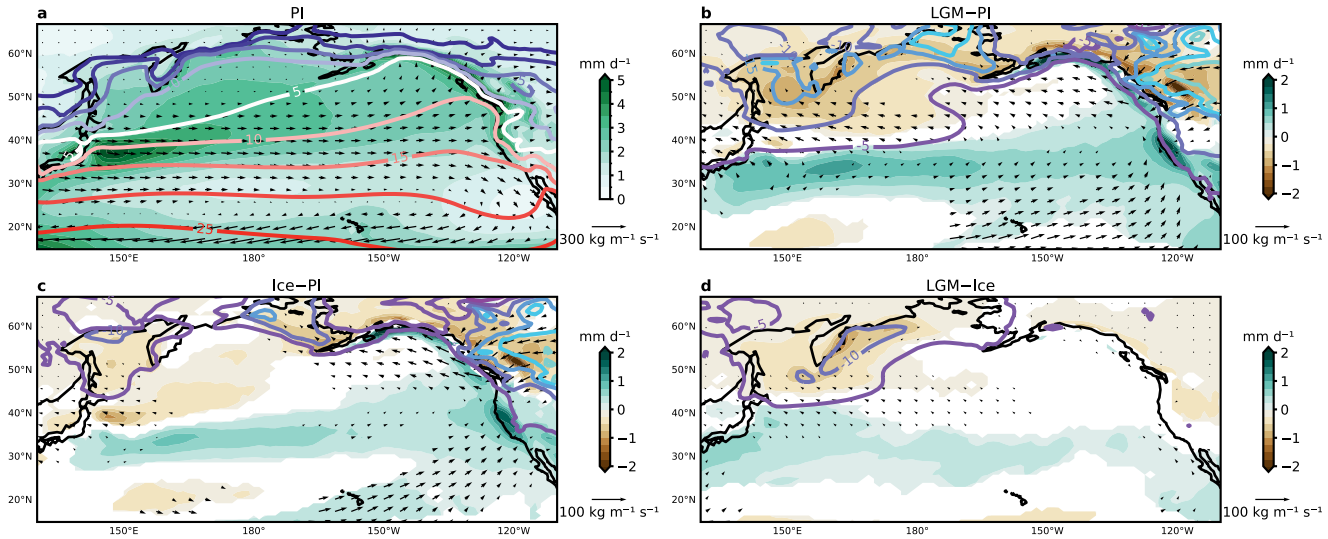

Figure 4. Non-AR cold-season moisture transport and precipitation over the North Pacific. Average atmospheric moisture transport (arrows) and precipitation (filled contours) *not* associated with ARs during the winter half-year (November–April; see also Figure S2 in Supporting Information S1) over the North Pacific. Also shown are near-surface average temperatures (unfilled contours, 5°C interval) over the winter half-year; all temperature difference contours shown in panels (b)–(d) are negative. Panels as in Figures 1a–1d.

The ice sheet forcing is responsible for large decreases in AR total and extreme precipitation fraction across the North Pacific, for the tripolar structure over the North Atlantic, and for decreases in the southern hemisphere, especially close to continents (Figure 3g). The decreases in AR contribution to extreme precipitation are especially notable around the ice sheets (western and eastern Canada, northwestern Europe, and Iberia), while the only substantial increase associated with the ice sheet forcing occurs over southern Iberia. However, the ice sheets do not induce significant changes to the AR contributions to total or extreme precipitation over the subtropical eastern North Pacific and into southwestern North America. Other LGM forcings lead to decreases in that region, as well as around the margins of the North Atlantic and in a more distributed fashion in the southern hemisphere (Figure 3h).

Curiously, the modest increase in LGM precipitation in southwestern North America is difficult to explain with our IVT and AR results. In particular, AR activity and associated precipitation both decrease over the eastern North Pacific in the LGM simulation (Figure 3b). This is largely a consequence of forcings other than the ice sheets (Figure 3d); in the case with only ice sheets, a broad region between Hawaii and California sees no significant change in AR activity (Figure 3c) despite lower atmospheric water vapor. Nevertheless, there is little indication of changes that would enhance precipitation, apart from increased land-sea temperature gradients (Figure 4) that enhance rainout upon landfall (Boos, 2012; Morrill et al., 2018; Tabor et al., 2021); this is in contrast to previous findings indicating stronger southwesterly moisture transport into southwestern North America at the LGM (Lora, 2018; Lora et al., 2017).

We find a significant increase in LGM cold-season precipitation in southwestern North America, particularly in coastal areas, that is *not* directly associated with ARs (Figure 4). This change, both in the ice sheet and full LGM simulations, results from a southward shift of non-AR extratropical precipitation, with decreases at high latitudes and most of the increases at subtropical latitudes (Figures 4b and 4c); an exception is along the coastlines at higher latitudes, where changes in temperature gradients, increased elevation, and more exposed land contribute to an enhanced rainout effect. Most of these changes can be attributed to forcing related to the ice sheet alone (Figure 4c), with the LGM configuration contributing a relatively minor additional southward shift, particularly in the western part of the North Pacific associated with lower temperatures from additional sea ice in the Bering and Okhotsk Seas (Figure 4d). Much of the precipitation increases in southwestern North America seem to be related to a modest increase in weak wintertime southerly or southwesterly moisture transport, bringing moist air from lower latitudes (Figures 4b and 4c). These enhancements are not associated with changes in seasonality (Figure S2 in Supporting Information S1), suggesting instead more frequent but less coherent moisture delivery taking the place of ARs. It should be noted, however, that non-AR precipitation over the continent need not

come exclusively from non-AR moisture transport, and can also be delivered in part by ARs that dissipate before reaching the coastline. Nevertheless, these results overall suggest a decrease in the average intensity of moisture transport events affecting southwestern North America, despite an overall increase in precipitation and its extremes (Figure 1).

While the North Pacific AR frequency decrease in our simulations agrees with the overall moisture transport and convergence changes (Figure 2), one can ask whether this AR response is artificially caused or amplified by the details of our AR detection algorithm; after all, the LGM is a strongly altered climate relative to the preindustrial. However, our algorithm is designed to account for changes in climate state; in addition, tests changing both the minimum IVT threshold and minimum length requirement in the algorithm produce the same result (not shown). Indeed, we conducted an extreme test wherein the algorithm restrictiveness was drastically lowered for the LGM simulation *but not for the preindustrial*, resulting in generally higher detections in the former simulation. Globally, this produced global increases in LGM AR activity (unphysical by design), *except* in the region in question, over the western North Pacific, where detected ARs decreased even under these incomparable requirements. We therefore conclude that it is indeed a feature of our simulations, and not our AR detection algorithm, that LGM North Pacific ARs consistently decrease. Whether this is a realistic response, or an inaccurate one resulting from too-high ice sheet topography or too-cold a climate (or some other model bias), remains an open question.

4. Discussion and Conclusions

We have investigated the behavior of precipitation and atmospheric moisture transport, and their extremes including ARs, in CESM2 simulations of the LGM climate. The LGM ice sheets elicit a strong response of the circulation in the northern mid-latitudes. This, in combination with atmospheric humidity decreases particularly in subtropical areas, leads to a southeastward shift of moisture transport and precipitation over both the North Atlantic and Pacific. Other LGM forcings, which further cool the atmosphere and strengthen temperature gradients over the North Atlantic, enhance these patterns and especially increase moisture convergence over the subpolar North Atlantic. In the southern hemisphere, the LGM forcings lead to generally weakened moisture transport resulting from equatorward shifts of winds and eddies, and from decreased humidity (see Figures S3–S5 in Supporting Information S1).

While we identify the LGM ice sheets as the dominant forcing in our simulations, in agreement with many previous results, it is worth emphasizing that our results do not imply that the responses to LGM forcings are linearly additive. In other words, the response of the climate system to lower greenhouse gases or an altered orbit could be different depending on the presence or absence of the ice sheets, and we have not investigated such sensitivities explicitly. Furthermore, we also have not specifically diagnosed whether the North American hydroclimate response to ice sheets, for example, is due to the direct steering of wintertime circulation or is mediated by North Pacific sea surface temperatures (though sea surface temperatures in our simulations are qualitatively consistent with those of Amaya et al. (2022)).

Mean and extreme precipitation over land generally decrease under LGM conditions, but robustly increase in three mid-latitude regions: Patagonia, Iberia, and southwestern North America. In the first of these, increased moisture convergence occurs due to lifting and enhanced rainout by local ice sheets, despite weakened IVT throughout the southern hemisphere. In the second, increased moisture convergence is driven by a constricted and zonalized North Atlantic atmospheric circulation, and associated enhanced AR activity. In the third, small, mainly southerly moisture transport increases onto the continent, interacting with strengthened temperature gradients, lead to modest enhancements of convergence and precipitation.

That the higher LGM precipitation over southwestern North America in our simulations is not clearly explained by increased southwesterly IVT or by enhanced AR activity over the southeastern North Pacific is curious, as it contradicts previous results from simulations employing PMIP3 LGM boundary conditions, in which ARs in the North Pacific robustly increased southwesterly moisture transport into southwestern North America (Lora et al., 2017). While some interpretations of proxy records suggest a more northerly LGM moisture source (Feakins et al., 2019; Oster et al., 2015), it is difficult to reconcile that with southward ice sheet-induced circulation shifts. Indeed, our simulations perhaps suggest more *southerly* flow (Figure 2b) than previous modeling results (Lora et al., 2017). Notably, the PMIP3 ice sheet reconstruction was lower than that used here and, indeed, the PMIP4 model ensemble (which includes simulations with these higher ice sheets) produces lower

precipitation over southwestern North America than the PMIP3 ensemble (see Fig. 6 of Kageyama et al., 2021). While the individual models in the two ensembles are quite different (and there are different numbers of models in each), this generally suggests that North American LGM precipitation, closely associated with circulation changes (Lora, 2018), depends sensitively on the details of the ice sheet.

Furthermore, while reconstructions generally agree that wetter LGM conditions occurred in western North America (e.g., Cleator et al., 2020; Kirby et al., 2013; Oster et al., 2015), it is by no means settled whether Iberia was truly a wetter region at the LGM. Proxy evidence exists suggesting both wetter and drier conditions there, though in all cases uncertainties are substantial and the proxy records difficult to interpret decisively (Bartlein et al., 2011; Beghin et al., 2016; Camuera et al., 2019; Cleator et al., 2020; Moreno et al., 2014). Multiple previous modeling results have suggested increased LGM precipitation in the western Mediterranean (Kageyama et al., 2021; Laîné et al., 2009; Löfverström & Lora, 2017), in agreement with our results. Nevertheless, whether a climatologically zonalized circulation or more episodic events associated with teleconnections in the LGM atmosphere (Lofverstrom, 2020) are dominantly responsible remains unresolved. The sensitivity of these changes to ice sheet topography and the level of model dependence involved are open questions, as is the degree to which changes in precipitation frequency and intensity translate into mean changes captured by proxies. Our results could inform regional proxy system models that address this latter issue, and could aid in interpreting the apparent discrepancies between Iberia and southwestern North America. Relatedly, model uncertainty remains high, yet we are limited in our analysis of other models' available results due to a lack of temporal resolution (daily or higher) for relevant fields. Attention to this gap is needed in order to expand our understanding of the responses of moisture transport and hydroclimate extremes to past climate states, and to connect them with the underlying synoptic processes that produce them, and the proxies that record them.

Data Availability Statement

CESM2 model code is available at https://www.cesm.ucar.edu/models/cesm2/release_download.html. Processed simulation data needed to reproduce our figures are archived and publicly available on Zenodo at https://doi.org/10.5281/zenodo.8327272, and additional data from the LGM and PI control simulations are available on Zenodo at https://doi.org/10.5281/zenodo.7339985.

Acknowledgments
This work was funded by National Science Foundation Awards AGS-1903528, AGS-1903600, and EAR-2102853. The CESM project is supported primarily by the National Science Foundation (NSF). This material is based upon work supported by the National Center for Atmospheric Research, which is a major facility sponsored by the NSF under Cooperative Agreement No. 1852977. Computing and data storage resources, including the Cheyenne supercomputer (http://doi.org/10.5065/D6RX99HX), were provided by the Computational and Information Systems Laboratory (CISL) at NCAR. We also gratefully acknowledge the Yale Center for Research Computing.

References

Amaya, D. J., Seltzer, A. M., Karnauskas, K. B., Lora, J. M., Zhang, X., & DiNezio, P. N. (2022). Air-sea coupling shapes North American hydroclimate response to ice sheets during the Last Glacial Maximum. *Earth and Planetary Science Letters*, *578*, 117271. https://doi.org/10.1016/j.epsl.2021.117271

Annan, J. D., Hargreaves, J. C., & Mauritsen, T. (2022). A new global surface temperature reconstruction for the Last Glacial Maximum. *Climate of the Past*, *18*(8), 1883–1896. https://doi.org/10.5194/cp-18-1883-2022

Baek, S. H., Battalio, J. M., & Lora, J. M. (2023). Atmospheric river variability over the Last Millennium driven by annular modes. *AGU Advances*, *4*(1), e2022AV000834. https://doi.org/10.1029/2022av000834

Baek, S. H., & Lora, J. M. (2021). Counterbalancing influences of aerosols and greenhouse gases on atmospheric rivers. *Nature Climate Change*, *11*, 958–965. https://doi.org/10.1038/s41558-021-01166-8

Bartlein, P. J., Harrison, S. P., Brewer, S., Connor, S., Davis, B. A. S., Gajewski, K., et al. (2011). Pollen-based continental climate reconstructions at 6 and 21 ka: A global synthesis. *Climate Dynamics*, *37*(3–4), 775–802. https://doi.org/10.1007/s00382-010-0904-1

Beghin, P., Charbit, S., Kageyama, M., Combourieu-Nebut, N., Hatté, C., Dumas, C., & Peterschmitt, J.-Y. (2016). What drives LGM precipitation over the western Mediterranean? A study focused on the Iberian Peninsula and northern Morocco. *Climate Dynamics*, *46*(7–8), 2611–2631. https://doi.org/10.1007/s00382-015-2720-0

Boos, W. R. (2012). Thermodynamic scaling of the hydrological cycle of the Last Glacial Maximum. *Journal of Climate*, *25*(3), 992–1006. https://doi.org/10.1175/jcli-d-11-00010.1

Broecker, W. (2010). Long-term water prospects in the western United States. *Journal of Climate*, *23*(24), 6669–6683. https://doi.org/10.1175/2010jcli3780.1

Camuera, J., Jiménez-Moreno, G., Ramos-Román, M., García-Alix, A., Toney, J. A., Anderson, R. S., et al. (2019). Vegetation and climate changes during the last two glacial-interglacial cycles in the western Mediterranean: A new long pollen record from Padul (southern Iberian Peninsula). *Quaternary Science Reviews*, *205*, 86–105. https://doi.org/10.1016/j.quascirev.2018.12.013

Cleator, S. F., Harrison, S. P., Nichols, N. K., Prentice, I. C., & Roulstone, I. (2020). A new multivariable benchmark for Last Glacial Maximum climate simulations. *Climate of the Past*, *16*(2), 699–712. https://doi.org/10.5194/cp-16-699-2020

Cook, K. H., & Held, I. M. (1988). Stationary waves of the Ice Age climate. *Journal of Climate*, *1*(8), 807–819. https://doi.org/10.1175/1520-0442(1988)001<0807:swotia>2.0.co;2

Danabasoglu, G., Lamarque, J.-F., Bacmeister, J., Bailey, D. A., DuVivier, A. K., Edwards, J., et al. (2020). The Community Earth System model Version 2 (CESM2). *Journal of Advances in Modeling Earth Systems*, *12*, e2019MS001916. https://doi.org/10.1029/2019ms001916

Dettinger, M. D., Ralph, F. M., Das, T., Neiman, P. J., & Cayan, D. R. (2011). Atmospheric rivers, floods and the water resources of California. *Water*, *3*(2), 445–478. https://doi.org/10.3390/w3020445

DiNezio, P. N., Tierney, J. E., Otto-Bliesner, B. L., Timmermann, A., Bhattacharya, T., Rosenbloom, N., & Brady, E. (2018). Glacial changes in tropical climate amplified by the Indian Ocean. *Science Advances*, *4*(12), eaat965. https://doi.org/10.1126/sciadv.aat9658

Donohoe, A., & Battisti, D. S. (2009). Causes of reduced North Atlantic storm activity in a CAM3 simulation of the last glacial maximum. *Journal of Climate*, *22*(18), 4793–4808. https://doi.org/10.1175/2009jcli2776.1

Feakins, S. J., Wu, M. S., Ponton, C., & Tierney, J. E. (2019). Biomarkers reveal abrupt switches in hydroclimate during the last glacial in southern California. *Earth and Planetary Science Letters*, *515*, 164–172. https://doi.org/10.1016/j.epsl.2019.03.024

Goldsmith, Y., Polissar, P., Ayalon, A., Bar-Matthews, M., Demenocal, P., & Broecker, W. S. (2017). The modern and Last Glacial Maximum hydrological cycles of the Eastern Mediterranean and the Levant from a water isotope perspective. *Earth and Planetary Science Letters*, *457*, 303–312. https://doi.org/10.1016/j.epsl.2016.10.017

Guan, B., Molotch, N. P., Waliser, D. E., Fetzer, E. J., & Neiman, P. J. (2010). Extreme snowfall events linked to atmospheric rivers and surface air temperature via satellite measurements. *Geophysical Research Letters*, *37*(20), L20401. https://doi.org/10.1029/2010gl044696

Held, I. M., & Soden, B. J. (2006). Robust responses of the hydrological cycle to global warming. *Journal of Climate*, *19*(21), 5686–5699. https://doi.org/10.1175/jcli3990.1

Kageyama, M., Harrison, S. P., Kapsch, M.-L., Lofverstrom, M., Lora, J. M., Mikolajewicz, U., et al. (2021). The PMIP4 Last Glacial Maximum experiments: Preliminary results and comparison with the PMIP3 simulations. *Climate of the Past*, *17*(3), 1065–1089. https://doi.org/10.5194/cp-17-1065-2021

Kageyama, M., & Valdes, P. J. (2000). Impact of the North American ice-sheet orography on the last glacial maximum eddies and snowfall. *Geophysical Research Letters*, *27*(10), 1515–1518. https://doi.org/10.1029/1999gl011274

Kirby, M. E., Feakins, S. J., Bonuso, N., Fantozzi, J. M., & Hiner, C. A. (2013). Latest Pleistocene to Holocene hydroclimates from Lake Elsinore, California. *Quaternary Science Reviews*, *76*, 1–15. https://doi.org/10.1016/j.quascirev.2013.05.023

Kutzbach, J. E., & Wright, H. E. (1985). Simulation of the climate of 18,000 yr BP: Results for the North American/North Atlantic/European sector and comparison with the geologic record. *Quaternary Science Reviews*, *4*(3), 147–187. https://doi.org/10.1016/0277-3791(85)90024-1

Laîné, A., Kageyama, M., Salas-Mélia, D., Voldoire, A., Rivière, G., Ramstein, G., et al. (2009). Northern hemisphere storm tracks during the Last Glacial Maximum in the PMIP2 ocean-atmosphere coupled models: Energetic study, seasonal cycle, precipitation. *Climate Dynamics*, *32*(5), 593–614. https://doi.org/10.1007/s00382-008-0391-9

Lamjiri, M. A., Dettinger, M. D., Ralph, F. M., & Guan, B. (2017). Hourly storm characteristics along the U.S. West Coast: Role of atmospheric rivers in extreme precipitation. *Geophysical Research Letters*, *44*(13), 7020–7028. https://doi.org/10.1002/2017gl074193

Lavers, D. A., & Villarini, G. (2013). The nexus between atmospheric rivers and extreme precipitation across Europe. *Geophysical Research Letters*, *40*(12), 3259–3264. https://doi.org/10.1002/grl.50636

Lee, H.-I., Mitchell, J. L., Lora, J. M., & Tripati, A. (2023). Influence of stationary waves on precipitation change in North American summer during the Last Glacial Maximum. *Journal of Climate*, *36*(10), 3165–3182. https://doi.org/10.1175/jcli-d-21-0886.1

Li, C., & Battisti, D. S. (2008). Reduced Atlantic storminess during the Last Glacial Maximum: Evidence from a coupled climate model. *Journal of Climate*, *21*(14), 3561–3579. https://doi.org/10.1175/2007jcli2166.1

Lofverstrom, M. (2020). A dynamic link between high-intensity precipitation events in southwestern North America and Europe at the Last Glacial Maximum. *Earth and Planetary Science Letters*, *534*, 116081. https://doi.org/10.1016/j.epsl.2020.116081

Löfverström, M., Caballero, R., Nilsson, J., & Messori, G. (2016). Stationary wave reflection as a mechanism for zonalizing the Atlantic winter jet at the LGM. *Journal of the Atmospheric Sciences*, *73*(8), 3329–3342. https://doi.org/10.1175/jas-d-15-0295.1

Löfverström, M., & Lora, J. M. (2017). Abrupt regime shifts in the North Atlantic atmospheric circulation over the last deglaciation. *Geophysical Research Letters*, *44*(15), 8047–8055. https://doi.org/10.1002/2017gl074274

Lora, J. M. (2018). Components and mechanisms of hydrologic cycle changes over North America at the Last Glacial Maximum. *Journal of Climate*, *31*(17), 7035–7051. https://doi.org/10.1175/jcli-d-17-0544.1

Lora, J. M., Mitchell, J. L., Risi, C., & Tripati, A. E. (2017). North Pacific atmospheric rivers and their influence on western North America at the Last Glacial Maximum. *Geophysical Research Letters*, *44*(2), 1051–1059. https://doi.org/10.1002/2016gl071541

Lora, J. M., Shields, C. A., & Rutz, J. J. (2020). Consensus and disagreement in atmospheric river detection: ARTMIP global catalogues. *Geophysical Research Letters*, *47*(20), e2020GL089302. https://doi.org/10.1029/2020gl089302

Marquardt Collow, A. B., Shields, C. A., Guan, B., Kim, S., Lora, J. M., McClenny, E. E., et al. (2022). An overview of ARTMIP's Tier 2 reanalysis intercomparison: Uncertainty in the detection of atmospheric rivers and their associated precipitation. *Journal of Geophysical Research: Atmospheres*, *127*(8), e2021JD036155. https://doi.org/10.1029/2021jd036155

Menemenlis, S., Lora, J. M., Lofverstrom, M., & Chandan, D. (2021). Influence of stationary waves on mid-Pliocene atmospheric rivers and hydroclimate. *Global and Planetary Change*, *204*, 103557. https://doi.org/10.1016/j.gloplacha.2021.103557

Merz, N., Raible, C. C., & Woollings, T. (2015). North Atlantic eddy-driven jet in interglacial and glacial winter climates. *Journal of Climate*, *28*(10), 3977–3997. https://doi.org/10.1175/jcli-d-14-00525.1

Moreno, A., Svensson, A., Brooks, S. J., Connor, S., Engels, S., Fletcher, W., et al. (2014). A compilation of western European terrestrial records 60–8 ka BP: Towards an understanding of latitudinal climatic gradients. *Quaternary Science Reviews*, *106*, 167–185. https://doi.org/10.1016/j.quascirev.2014.06.030

Morrill, C., Lowry, D. P., & Hoell, A. (2018). Thermodynamic and dynamic causes of pluvial conditions during the Last Glacial Maximum in western North America. *Geophysical Research Letters*, *45*(1), 335–345. https://doi.org/10.1002/2017gl075807

Newman, M., Kiladis, G. N., Weickmann, K. M., Ralph, F. M., & Sardeshmukh, P. D. (2012). Relative contributions of synoptic and low-frequency eddies to time-mean atmospheric moisture transport, including the role of atmospheric rivers. *Journal of Climate*, *25*(21), 7341–7361. https://doi.org/10.1175/jcli-d-11-00665.1

O'Brien, T. A., Wehner, M. F., Payne, A. E., Shields, C. A., Rutz, J. J., Leung, L.-R., et al. (2022). Increases in future AR count and size: Overview of the ARTMIP Tier 2 CMIP5/6 experiment. *Journal of Geophysical Research: Atmospheres*, *127*(6), e2021JD036013. https://doi.org/10.1029/2021jd036013

O'Gorman, P. A., & Schneider, T. (2008). The hydrological cycle over a wide range of climates simulated with an idealized GCM. *Journal of Climate*, *21*(15), 3815–3832. https://doi.org/10.1175/2007jcli2065.1

Oster, J. L., Ibarra, D. E., Winnick, M. J., & Maher, K. (2015). Steering of westerly storms over western North America at the Last Glacial Maximum. *Nature Geoscience*, *8*(3), 201–205. https://doi.org/10.1038/ngeo2365

Paul, A., Mulitza, S., Stein, R., & Werner, M. (2021). A global climatology of the ocean surface during the Last Glacial Maximum mapped on a regular grid (GLOMAP). *Climate of the Past*, *17*(2), 805–824. https://doi.org/10.5194/cp-17-805-2021

Peltier, W. R., Argus, D. F., & Drummond, R. (2015). Space geodesy constrains ice-age terminal deglaciation: The global ICE-6G_C (VM5a) model. *Journal of Geophysical Research: Solid Earth*, *120*(1), 450–487. https://doi.org/10.1002/2014jb011176

Pinto, J. G., & Ludwig, P. (2020). Extratropical cyclones over the North Atlantic and western Europe during the last glacial maximum and implications for proxy interpretation. *Climate of the Past*, *16*(2), 611–626. https://doi.org/10.5194/cp-16-611-2020

Ralph, F. M., Rutz, J. J., Cordeira, J. M., Dettinger, M., Anderson, M., Reynolds, D., et al. (2019). A scale to characterize the strength and impacts of atmospheric rivers. *Bulletin America Meteorology Social*, *46*, 1814–1823.

Rivière, G., Berthou, S., Lapeyre, G., & Kageyama, M. (2018). On the reduced North Atlantic storminess during the Last Glacial Period: The role of topography in shaping synoptic eddies. *Journal of Climate*, *31*(4), 1637–1652. https://doi.org/10.1175/jcli-d-17-0247.1

Rivière, G., Laîné, A., Lapeyre, G., Salas-Mélia, D., & Kageyama, M. (2010). Links between Rossby wave breaking and the North Atlantic Oscillation–Arctic Oscillation in present-day and Last Glacial Maximum climate simulations. *Journal of Climate*, *23*(11), 2987–3008. https://doi.org/10.1175/2010jcli3372.1

Roberts, W. H. G., Li, C., & Valdes, P. J. (2019). The mechanisms that determine the response of the Northern Hemisphere's stationary waves to North American ice sheets. *Journal of Climate*, *32*(13), 3917–3940. https://doi.org/10.1175/jcli-d-18-0586.1

Rutz, J. J., Shields, C. A., Lora, J. M., Payne, A. E., Guan, B., Ullrich, P., et al. (2019). The Atmospheric River Tracking Method Intercomparison Project (ARTMIP): Quantifying uncertainties in atmospheric river climatology. *Journal of Geophysical Research: Atmospheres*, *124*(24), 13777–13802. https://doi.org/10.1029/2019jd030936

Schär, C., Ban, N., Fischer, E. M., Rajczak, J., Schmidli, J., Frei, C., et al. (2016). Percentile indices for assessing changes in heavy precipitation events. *Climatic Change*, *137*(1–2), 201–216. https://doi.org/10.1007/s10584-016-1669-2

Scheff, J., Seager, R., Liu, H., & Coats, S. (2017). Are glacials dry? Consequences for paleoclimatology and for greenhouse warming. *Journal of Climate*, *30*(17), 6593–6609. https://doi.org/10.1175/jcli-d-16-0854.1

Shaw, T. A., Baldwin, M., Barnes, E. A., Caballero, R., Garfinkel, C. I., Hwang, Y.-T., et al. (2016). Storm track processes and the opposing influences of climate change. *Nature Geoscience*, *9*, 656–664. https://doi.org/10.1038/ngeo2783

Skinner, C. B., Lora, J. M., Payne, A. E., & Poulsen, C. J. (2020). Atmospheric river changes shaped mid-latitude hydroclimate since the mid-Holocene. *Earth and Planetary Science Letters*, *541*, 116293. https://doi.org/10.1016/j.epsl.2020.116293

Skinner, C. B., Lora, J. M., Tabor, C., & Zhu, J. (2023). Atmospheric river contributions to ice sheet hydroclimate at the Last Glacial Maximum. *Geophysical Research Letters*, *50*(1), e2022GL101750. https://doi.org/10.1029/2022gl101750

Sodemann, H., & Stohl, A. (2013). Moisture origin and meridional transport in atmospheric rivers and their association with multiple cyclones. *Monthly Weather Review*, *141*(8), 2850–2868. https://doi.org/10.1175/mwr-d-12-00256.1

Tabor, C., Lofverstrom, M., Oster, J., Wortham, B., de Wet, C., Montañez, I., et al. (2021). A mechanistic understanding of oxygen isotopic changes in the Western United States at the Last Glacial Maximum. *Quaternary Science Reviews*, *274*, 107255. https://doi.org/10.1016/j.quascirev.2021.107255

Tierney, J. E., Zhu, J., King, J., Malevich, S. B., Hakim, G. J., & Poulsen, C. J. (2020). Glacial cooling and climate sensitivity revisited. *Nature*, *584*(7822), 569–573. https://doi.org/10.1038/s41586-020-2617-x

Ullman, D. J., LeGrande, A. N., Carlson, A. E., Anslow, F. S., & Licciardi, J. M. (2014). Assessing the impact of Laurentide Ice Sheet topography on glacial climate. *Climate of the Past*, *10*(2), 487–507. https://doi.org/10.5194/cp-10-487-2014

Viale, M., Valenzuela, R., Garreaud, R. D., & Ralph, F. M. (2018). Impacts of atmospheric rivers on precipitation in South America. *Journal of Hydrometeorology*, *19*(10), 1671–1687. https://doi.org/10.1175/jhm-d-18-0006.1

Waliser, D., & Guan, B. (2017). Extreme winds and precipitation during landfall of atmospheric rivers. *Nature Geoscience*, *10*(3), 179–183. https://doi.org/10.1038/ngeo2894

Zhang, Z., Ralph, F. M., & Zheng, M. (2019). The relationship between extratropical cyclone strength and atmospheric river intensity and position. *Geophysical Research Letters*, *46*(3), 1814–1823. https://doi.org/10.1029/2018gl079071

Zhu, Y., & Newell, R. E. (1998). A proposed algorithm for moisture fluxes from atmospheric rivers. *Monthly Weather Review*, *21*, 152–158.